Journal of Constructional Steel Research 177 (2021) 106417

Contents lists available at ScienceDirect

Journal of Constructional Steel Research

Seismic design of non-dissipative embedded column base connections

Hiroyuki Inamasu [a], Amit M. Kanvinde [b], Dimitrios G. Lignos [a,*]

[a] Department of Architecture, Civil, Environmental Engineering, École Polytechnique Fédérale de Lausanne, Station 18, Lausanne 1015, Switzerland
[b] Department of Civil and Environmental Engineering, University of California, Davis, CA 95616, United States of America

ARTICLE INFO

Article history:
Received 5 June 2020
Received in revised form 18 September 2020
Accepted 13 October 2020
Available online 24 October 2020

Keywords:
Embedded column bases
Wide flange columns
Capacity design
Cyclic loading
Finite element model

ABSTRACT

Embedded Column Base (ECB) connections in seismically resistant steel moment frames are commonly designed to be stronger than the connected column, to protect them from inelastic actions. This relies on estimation of demands induced by the column and the strength capacity of the connections themselves. However, recent research indicates that prevalent approaches may be unconservative for both demand and capacity estimation, with the consequence of unintended damage/failure of the connection. Motivated by the above, this research (1) characterizes the seismic demands induced in ECB connections, and (2) evaluates various strength models for these connections, in support of improved design approaches. This is done through a virtual test program that uses validated continuum finite element simulations of interactive column-ECB subassemblies. The results suggest that the current design approaches for ECB connections are unconservative, i.e., they underestimate demands while also overestimating the ECB resistance, with the possibility of unintentional nonlinear behavior within the embedded portion of the ECB connection. This is undesirable, because the ECB connections are not usually detailed to provide plastic deformation capacity. A method is proposed to provide improved estimates of the anticipated flexural demands of non-dissipative ECB connections, along with recommendations regarding the strength models. To accomplish this, the method incorporates local cross-sectional slenderness, gravity-induced axial load demand in conjunction with load combinations imposed by current seismic design standards. The sensitivity to the steel column material grade, the imposed loading history, and axial load demands is studied, and limitations of the approach are outlined.

1. Introduction

Column base connections in steel moment-resisting frames (MRFs) withstand combinations of axial load, flexural and shear demands that are transferred to the foundation system during earthquake loading. While exposed column base connections are a standard practice in low-rise steel construction, embedded column bases (ECBs) are commonly used to achieve a fixed boundary condition at the lower end of first story steel columns in seismic resistant mid- to high-rise steel MRFs. Fig. 1 schematically illustrates a typical ECB detail, indicating its main components, including the steel column. The column is usually welded to a base plate that rests on a concrete layer for leveling of the steel column. The embedded portion of the steel column is encased by a reinforced concrete (RC) foundation. Face bearing plates are often employed at the top concrete layer to transfer axial compression and facilitate the formation of a shear panel. Referring to Fig. 1, the flexural resistance of non-dissipative ECB connections is provided through horizontal bearing of the column flanges as well as vertical bearing of the base plate and the face bearing plates.

In current design practice, it is commonly assumed that the steel column base portion above the RC footing is the dissipative element during an earthquake (through the formation of a column plastic hinge), whereas ECB connections themselves are non-dissipative (i.e., assumed to be brittle, and designed to be stronger than the attached column). The primary source of guidance for the strength-based design of these connections is the AISC Seismic Design Manual [1]. This follows a strength model, which was originally proposed for the design of a steel coupling beam bending within a concrete shear wall [2,3]. Despite of some similarities, this situation has significant differences with respect to ECB connections, including: (1) the absence of axial load in the coupling beam, which is present in the ECB column, (2) limited confinement in the thin shear wall, (3) the absence of the base plate, as well as differences in reinforcing bar patterns. As a result, the current design approaches are not directly applicable to ECB connections.

Moreover, in these as well as other approaches (e.g., [4]), it is commonly assumed that the ultimate flexural resistance of ECB connections is controlled by concrete bearing failure ahead of the compression flange of the column. Recent experiments and simulations [5] suggest that other failure modes are active as well – these include pryout of concrete on the tension side of the connection due to the uplift of the base plate, as well as cracking or failure in the web panel inside the RC

* Corresponding author.
E-mail address: dimitrios.lignos@epfl.ch (D.G. Lignos).

https://doi.org/10.1016/j.jcsr.2020.106417
0143-974X/

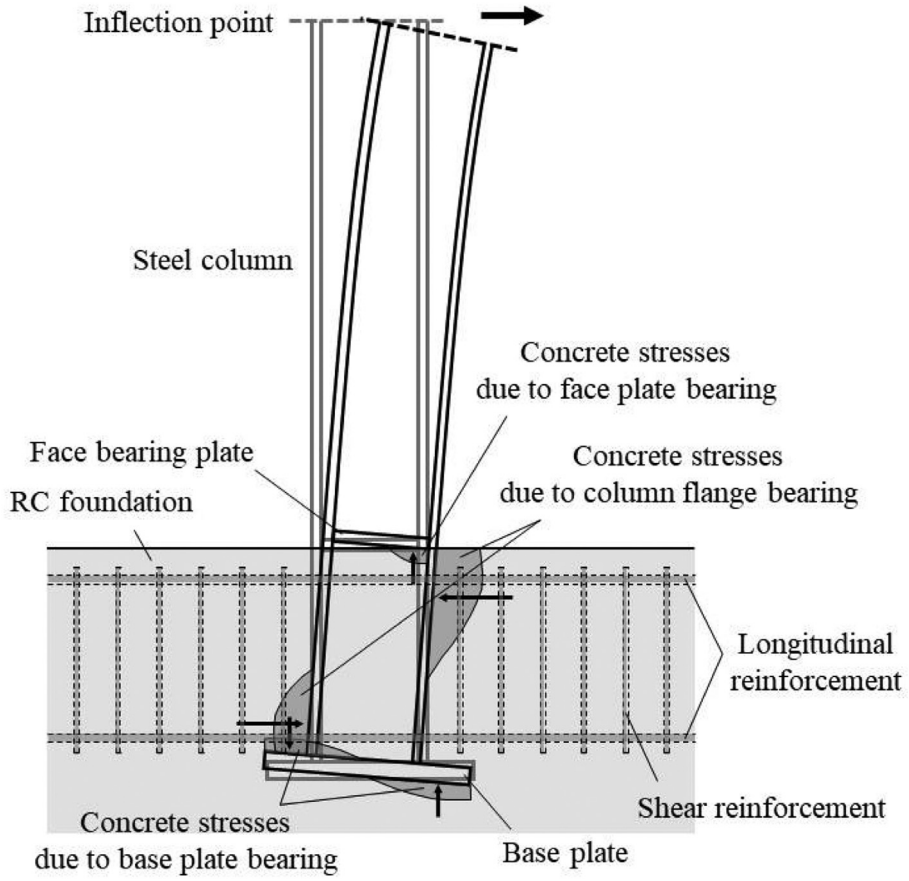

Fig. 1. Typical embedded column base connection detail and resisting mechanisms.

footing, further suggesting that the existing design guidance may be inadequate. These experiments also indicate that the behavior of ECB connections originates prior to reaching their assumed ultimate flexural resistance; this is due to gapping between the tension flange of the column and the adjacent concrete, as well as nonlinearity of the concrete on the bearing side adjacent to the compression flange. This is further corroborated by field observations from recent earthquakes [6,7] in which appreciable damage or inelastic behavior is noted in ECB connections, that are designed as non-dissipative (i.e., to be stronger than the adjoining column). Collectively, these experimental and field observations suggest that current methods for strength characterization of ECB connections may be inadequate, and quite possibly unconservative.

Similar concerns may also be noted on the demand side. Specifically, ECB connections are usually capacity-designed to develop the strain hardened capacity of the column – usually, this is determined as 1.1 times the expected full-plastic resistance of the column for A992 Gr. 50 (i.e., nominal yield stress, $f_{y,\,n} = 345$MPa). However, research on the inelastic behavior of wide-flange steel columns under multi-axis cyclic loading [8–12] suggests that the steel column force demands may be significantly higher than the above estimate. Moreover, the column force demands are strongly influenced by (a) the steel material cyclic hardening; (b) the loading conditions (i.e., coupled axial load and lateral drift demands); and (c) the cross-sectional slenderness that controls the onset of local buckling. However, the influence of the above parameters has not been considered in the seismic design process of ECB connections. Finally, although assumed to be fixed, ECB connections exhibit significant rotational flexibility [5,13–21], contributing to as much as 0.4–0.8% to the first story lateral drift demands.

Motivated by these issues, the main objectives of this paper are to: (1) critically examine the assumptions commonly used to design ECB connections, focusing on both capacity and demand assessment, and (2) provide recommendations for improved design of non-dissipative ECB connections. To achieve these objectives, the paper first reviews the current state-of-the-art in terms of the seismic design of non-dissipative ECB connections. This is accomplished by direct comparisons with pertinent experimental data available in the literature. Subsequently, the expected seismic demands of typical ECB connections are quantified through Continuum Finite Element (CFE) analyses of a virtual test matrix. A validated CFE model is used for this purpose. Within the virtual test matrix, several parameters, that may affect the seismic demands of ECB connections, are interrogated. The findings are synthesized into coherent recommendations for the seismic design of non-dissipative ECB connections in seismic resistant steel MRFs.

2. Review of prevalent strength models in the United States and Japan

The current AISC provisions [22] and the Design Manual [1] adapt the flexural/shear resistance of a steel coupling beam embedded to an RC wall for the seismic design of non-dissipative ECB connections. The stress block distributions, which are shown in Fig. 2a, are employed for this purpose. Concrete bearing controls the design shear resistance of the ECB connection, which may be computed as follows,

$$V_{Rd,AISC}^{ECB} = 4.04\sqrt{f'_c}\cdot\left(\frac{b_w}{b_f}\right)^{0.66}\cdot\beta_1\cdot b_f\cdot d_{embed}\cdot\left(\frac{0.58-0.22\cdot\beta_1}{0.88+\frac{L}{d_{embed}}}\right) \quad (1)$$

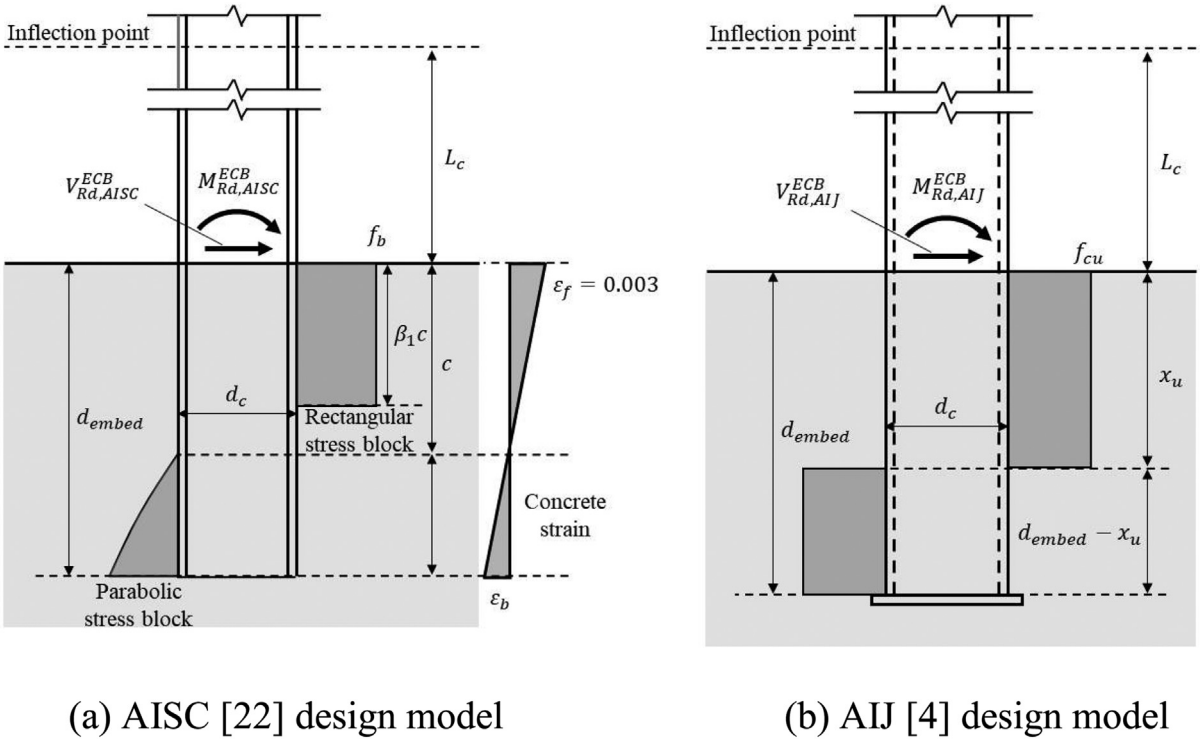

Fig. 2. Available design models for non-dissipative embedded column base connections.

The corresponding flexural resistance of an ECB connection may then be estimated as follows,

$$M^{ECB}_{Rd,AISC} = V^{ECB}_{Rd,AISC} \cdot L_c \tag{2}$$

In Eq. (1), f_c' is the specified concrete compressive strength (in MPa); b_w (in mm) is the width of the concrete foundation perpendicular to the plane of bending; b_f (in mm) is the column flange width; L_c is the distance from the top surface of the RC foundation to the inflection point of the column (in mm); β_1 is a factor relating the depth of the equivalent rectangular compressive stress block to the neutral axis depth as defined in [23]; and d_{embed} is the embedment depth of the steel column. In Eq. (1), the term $(b_w/b_f)^{0.66}$ accounts for the confinement effect of the concrete. Referring to Fig. 2a, f_b is the assumed maximum bearing stress of the concrete; c is the distance from the concrete top surface to the neutral axis in the assumed stress distribution; ε_f and ε_b are the assumed concrete strain demands at the top and bottom of the embedded portion of the column.

Grilli and Kanvinde [24] indicated that Eq. (1) does not consider the base plate contribution to the overall shear resistance of the ECB connection (see Fig. 1). Moreover, the term reflecting the effect of confinement on the corresponding bearing stress is unbounded. Accordingly, they introduced two factors, namely α and β to account for the base plate contribution to the shear resistance of ECB connections and the concrete confinement, respectively. While the former (see Eq. (3)) varies with respect to the embedment depth, d_{embed}, and the reference depth, d_{ref} (see Eq. (4)), the latter is assumed to be constant and equal to 2.0 after following the work of [25,26]. As such, the flexural resistance of a non-dissipative ECB connection should be computed as follows,

$$\alpha = 1 - \frac{d_{embed}}{d_{ref}} \tag{3}$$

$$d_{ref} = \frac{C}{\left(\frac{F}{4 \cdot E_s \cdot I}\right)^{\frac{1}{4}}} \tag{4}$$

$$d_{effective} = d_{ref} \leq d_{embed} \tag{5}$$

$$M^{ECB}_{Rd,Grilli} = \frac{1}{1-\alpha}\left[\beta \cdot \beta_1 \cdot f'_c \cdot b_j \cdot \left\{ d_L \cdot d_{effective} - \frac{\left(d_L^2 + d_U^2\right)}{2} \right\}\right] \tag{6}$$

In which, b_j is equal to $(b_f + B)/2$ and accounts for the concrete compression field outside the panel zone (in which, B is the base plate width as shown in Fig. 1); E_s and E_c are the Young's modulus of the steel and concrete materials, respectively; I, is the second moment of inertia of the steel column with respect to the direction of lateral loading. In Eq. (4), C is an empirical factor, assumed equal to 1.77. Referring to Fig. 1, the parameters, d_L and d_U are the depths of the lower and upper horizontal concrete bearing equivalent rectangular stress blocks, respectively. These may be determined by solving the force (i.e., shear and bending) equilibrium equations of the steel column inside the RC footing. Grilli and Kanvinde [24] proposed that the maximum horizontal bearing resistance is determined when $d_L + d_U$ reaches 60% of the effective embedment depth.

The AIJ [4] design provisions rely on the concrete bearing to estimate the flexural resistance of ECB connections. Referring to Fig. 2b, depending on the assumed stress distribution, a designer may either estimate the flexural resistance at yield or at ultimate (peak) of the respective ECB. The latter may be employed in the seismic design process of non-dissipative ECB connections in steel MRFs. This may be estimated as follows,

$$M^{ECB}_{Rd,AIJ} = f_{cu} \cdot B_c \cdot L_c \cdot \left\{ \sqrt{(2L_c + d_{embed})^2 + d_{embed}^2} - (2L_c + d_{embed}) \right\} \tag{7}$$

In which, f_{cu} is the maximum bearing strength, assumed equal to the specified concrete compressive strength f_c'; B_c is the column width (i.e., equal to b_f for wide flange cross-sections). In Fig. 2b, x_u is the distance from the concrete top surface to the neutral axis in the assumed stress distribution. While hollow structural sections are more common in the Japanese steel construction, Eq. (7) was originally developed

based on experimental work on ECBs featuring wide flange steel columns [13,14,18,19,21,27]. These represented interior steel MRF columns. In exterior column ECB connections, the AIJ [4] design provisions recommend specification of reinforcing bars where horizontal bearing concrete compressive stresses are expected to be large.

3. Available experimental data and assessment of current design models

To assess the efficacy of various capacity design approaches, forty-nine physical experiments on ECB connections featuring interior wide flange steel columns available in the literature were reviewed [5,13,15,18,19,21,27,28]. In 11 out of these 49 tests, the steel column remained elastic. The peak flexural/shear resistance of these ECBs were determined by concrete bearing, which is consistent with the assumed failure mode by the two aforementioned design models. However, the final failure mode in some of the available experimental data was associated with pryout at large lateral drift demands. Table 1 summarizes these tests including their key characteristics. Three specimens tested by Grilli et al. (#1, #2 and #4) were subjected to axial load in addition to lateral cyclic loading. However, the influence of axial load on the ECB response was not found to be important [5].

Fig. 3 depicts the typical hysteretic behavior of ECB connections from a prior test (i.e., Test #3) of the experimental program by [5]. The figure illustrates the base moment M_{base} versus the column drift ratio, θ. Several quantities of interest are extracted from this figure – namely, the maximum attained moment, $M_{max,\,p}$ and $M_{max,\,n}$ (positive and negative, respectively), and column drift ratio corresponding to M_{max} [= max ($|M_{max,\,p}|$,$|M_{max,\,n}|$)], θ_{max}; the effective elastic stiffness, K_e, which is defined as the secant stiffness using the point when M_{base} firstly reaches $M_y = 0.7M_{max}$; the yield rotation, θ_y, defined as the column drift ratio at M_y, the maximum attained moment of the ECB: $M_{max}^{ECB} = M_{max}$; and the yield moment of the ECB: $M_y^{ECB} = M_y$. The corresponding rotations of the ECB, θ_{max}^{ECB}, and, θ_y^{ECB},are deduced by subtracting the

Table 1
Experiments on ECB connections

Reference	ID	Column cross section (mm) ($d_c \times b_f \times t_w \times t_f$)[a]	d_{embed}/d_c	Foundation size (mm) ($b_w \times h_f \times l_f$)[b]	Concrete compressive strength f_c'(MPa)	Axial load[c] (kN)
Washio et al. [21]	POSALI	125 × 125 × 7 × 9	1.0	300 × 500 × 1300	25.3	0
Washio et al. [21]	POSAHI	125 × 125 × 7 × 9	1.0	300 × 500 × 1300	35.0	0
Washio et al. [21]	POTALI	125 × 125 × 7 × 9	1.0	300 × 500 × 1300	25.3	0
Minami et al. [14]	LA20	200 × 100 × 5.5 × 8	1.0	400 × 600 × 1600	20.6	0
Minami et al. [14]	LA10	200 × 100 × 5.5 × 8	0.5	400 × 600 × 1600	20.6	0
Takeda and Takahashi [19]	S2NO	250 × 100 × 9 × 19	1.0	1000 × 600 × 2800	16.2	0
Akiyama et al. [13]	ES-C	200 × 200 × 8 × 12	1.1	410 × 800 × 2750	20.0	0
Grilli et al. [5]	#1	455 × 418 × 42 × 68	1.1	1830 × 1092 × 3650	29.2	445
Grilli et al. [5]	#2	566 × 305 × 39 × 70	0.9	1830 × 1092 × 3650	29.2	445
Grilli et al. [5]	#3	455 × 418 × 42 × 68	1.7	1830 × 840 × 3650	29.2	0
Grilli et al. [5]	#4	455 × 418 × 42 × 68	1.7	1830 × 840 × 3650	29.2	445

[a] d_c, b_f, t_w, and t_f denote the depth, width, web thickness, and flange thickness of the column, respectively.
[b] b_w, h_f and l_f denote the width, height and length of concrete foundation, respectively.
[c] Positive value indicates compressive load.

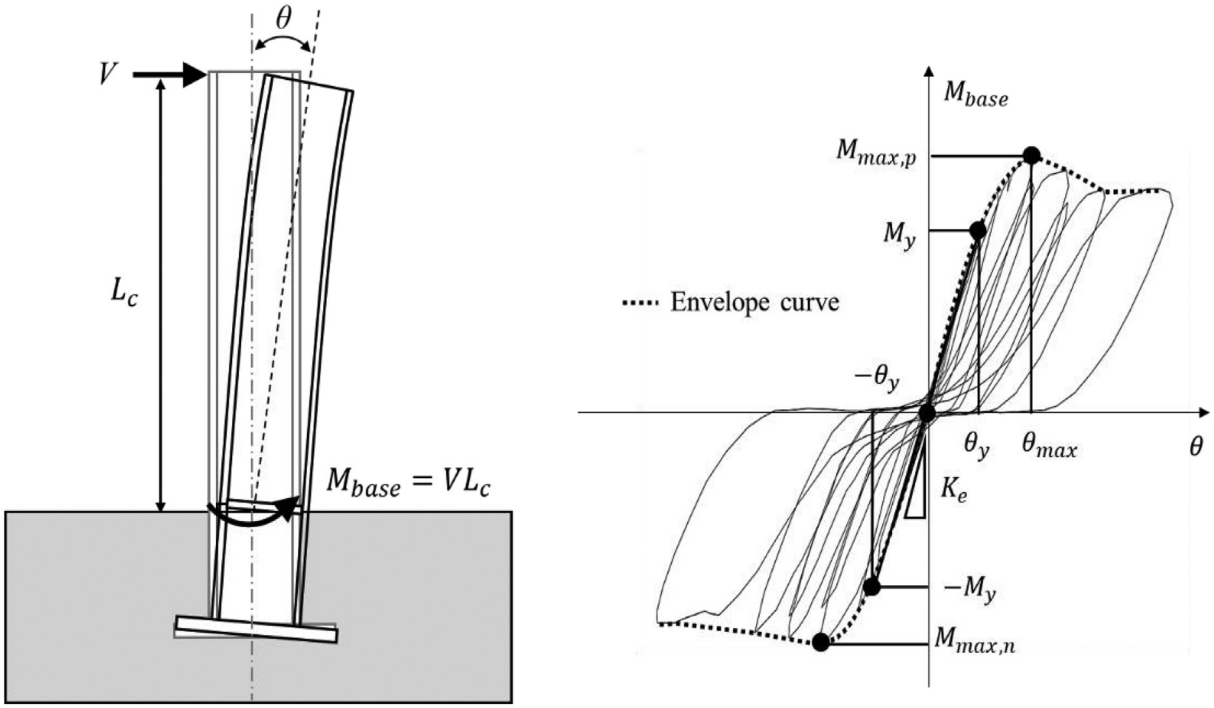

Fig. 3. Typical hysteretic behavior of embedded column bases along with the response parameters of interest.

elastic deformations due to flexure and shear of the column from θ_{max} and θ_y, respectively. The pre-capping plastic rotation of the ECB, θ_p^{ECB} is defined as the difference between θ_{max}^{ECB} and θ_y^{ECB}.

Fig. 4a shows a comparison of the measured maximum attained ECB moment, M_{max}^{ECB}, versus the model prediction, M_{Rd}^{ECB}, from Eqs. (2), (6) and (7) for the 11 test specimens, which are summarized in Table 1. In all cases, the cover concrete is considered part of the embedment depth as suggested in prior studies [2,3,29]. The established comparisons suggest that, in most cases, the AIJ [4] model underestimates the test results by at least a factor of two (average test-predicted ratio 3.20, with a Coefficient of Variation 0.40), whereas the AISC design model [1,22] yields more reasonable predictions (average test-predicted ratio 1.27, Coefficient of Variation 0.17). The AIJ model seems conservative because both the effect of concrete confinement on the bearing stress capacity as well as the contribution of the base plate are conservatively neglected. For five of the test specimens, the AISC model underestimates the attained ECB flexural resistance by 40 to 50%. This may be attributed to the fact that the base plate contribution to the ECB's lateral resistance is neglected. Referring to Fig. 4a, the accuracy of the Grilli and Kanvinde model [24] is noteworthy excluding one case (i.e., Specimen S2NO), in which the associated error is about 65%. This test specimen featured foundation beams perpendicular to the loading direction, thereby increasing the effective width, as well as the confinement of the concrete foundation compared to the remainder of the test specimens.

Although the data shown in Fig. 4a corresponds to the peak flexural resistance of the ECB connection, Grilli and Kanvinde [24] suggested that the yield flexural resistance, M_y^{ECB}, of an ECB connection may be assumed equal to $0.70M_{max}^{ECB}$ as a suitable estimate of the design resistance – this is because the connection exhibits significant nonlinearity after this point is reached. The gathered data, including the ones by [24], suggest that the corresponding $M_{y,\,deduced}^{ECB}/M_{max}^{ECB}$ ($M_{y,\,deduced}^{ECB}$ denotes the ECB moment at a tangent stiffness corresponding to 30% of the elastic stiffness of the footing) ratio is, on average, about 0.65 with a standard deviation of 0.08. This is depicted in Fig. 4b in which, the $M_{y,\,deduced}^{ECB}/M_{max}^{ECB}$ ratio is extracted directly from each one of the gathered test specimens. This is even more concerning especially when the prediction of the maximum flexural strength of ECBs is accurate, because it amplifies the unconservativeness of current methods for design, which rely on the ultimate resistance of the ECB connection.

4. Assessment of embedded column base design procedures through virtual testing

4.1. Development of finite element model

Referring to the preceding discussion, it is evident that both the demand as well as the capacity assessment methods implicit in the current design methods are inadequate from the standpoint of meeting design objectives (i.e., ensuring elastic response of the ECB connection). Because the overall performance depends on the interactions between the column as well as the ECB connection, it is informative to directly simulate these interactions. For this purpose, a CFE model is developed to simulate the cyclic behavior of wide flange steel columns embedded into RC footings. The CFE model is developed in the commercial software ABAQUS (version 6.14–1) [30]. A schematic illustration of the CFE model is shown in Fig. 5a. In brief, the steel column is modelled by shell elements with reduced order integration (S4R), while the ECB hysteretic behavior is condensed in a rotational spring at the bottom of the column that is tied to the bottom surface of the column. The hysteretic behavior of this spring is discussed hereinafter. The column top rotational spring represents the top end in-plane boundary condition of a first story column in capacity-designed steel MRFs. Details on how to derive the flexibility of the top end spring are discussed in [31]. The CFE model is parametrized and may easily be shifted to a cantilever column, by setting the top end spring's in-plane rotational stiffness to zero and by considering the proper member length. The CFE model is validated with available full-scale physical data on wide flange steel columns [8] as well as embedded column base connections [5]. The boundary conditions mimic the ones from the experimental setup of Suzuki and Lignos (2015) [8] and Grilli et al. (2017) [5]. The former employs cantilever columns, which are loaded with respect to the strong axis cross-sectional orientation. The column bottom is fixed in all six DOFs, whereas the column top end is only fixed in the out-plane direction in the displacement and rotational DOFs due to the lateral bracing system. In Grilli et al. (2017) [5], each specimen consists of a cantilever column with an ECB connection. Similarly, only in-plane movement was allowed in the test.

With regard to the wide flange steel columns, the CFE modelling strategy follows the general modelling recommendations by [11,12,32]. The CFE model features the Voce-Chaboche nonlinear multi-axial

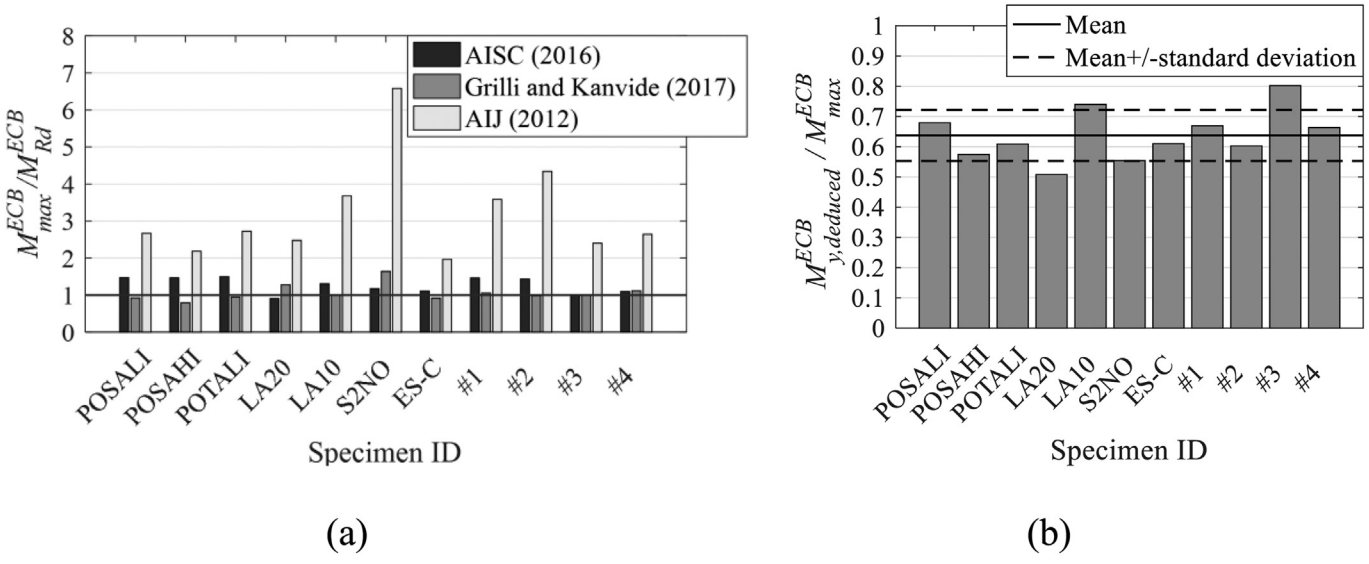

Fig. 4. Comparison of flexural strength of ECBs with gathered experimental data: (a) available peak flexural resistance, M_{max}^{ECB}, (b) yield flexural resistance, $M_{y,\,deduced}^{ECB}$.

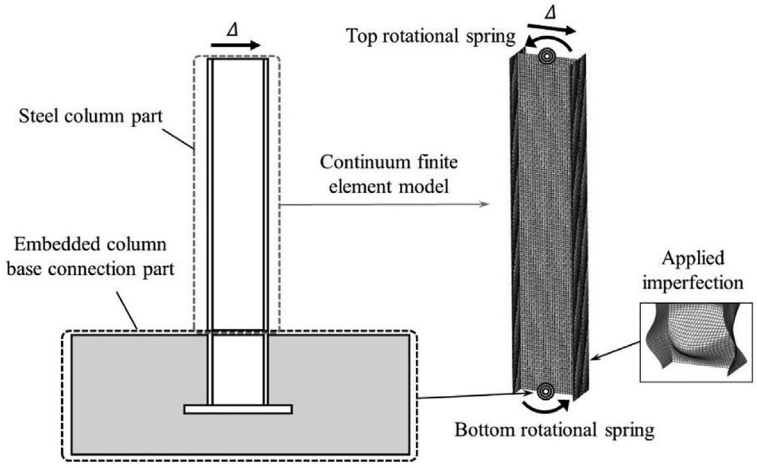

(a) Schematic illustration of developed CFE model

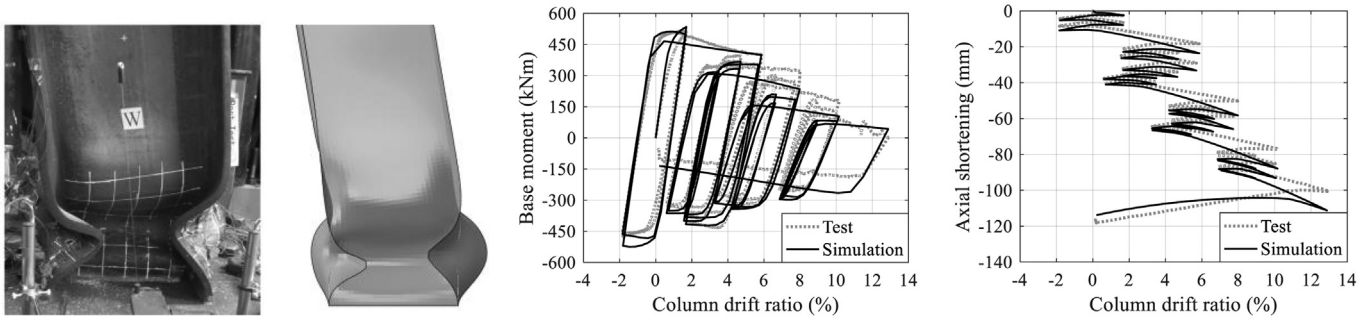

(b) Model validation of the steel column part: constant compressive axial load demands

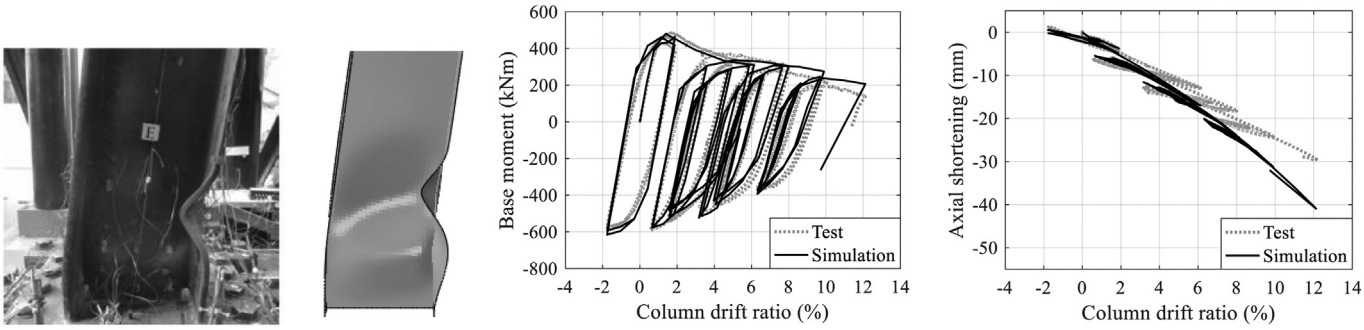

(c) Model validation of steel column part: variable axial load demands

Fig. 5. CFE model development and its validation (test data retrieved from [8]).

plasticity law [33,34]. The material model relies on consistent parameters calibrated through a gradient-based optimization based on work by [35,36]. Residual stresses due to hot-rolling are considered based on the residual stress distribution proposed by [37]. This is confirmed by recent residual stress measurements on hot-rolled wide flange profiles [38]. An idealized fixed-base column may be considered if the in-plane rotational spring of the column base is made infinite. In the CFE model, local buckling is triggered by considering local imperfections with a magnitude, which is smaller than the allowable manufacturing tolerance of hot-rolled profiles. Indicative values for these imperfections are discussed in [11,12].

The model validations constitute physical testing conducted by the last author and his former students [8,12] in which fixed-end cantilever specimens were subjected to a range of multi-axial cyclic loading histories. Fig. 5 shows indicative comparisons with such experiments with emphasis on tests subjected to collapse-consistent loading histories coupled with either compressive or time-varying axial load demands. From the same figure, the agreement between the simulated and

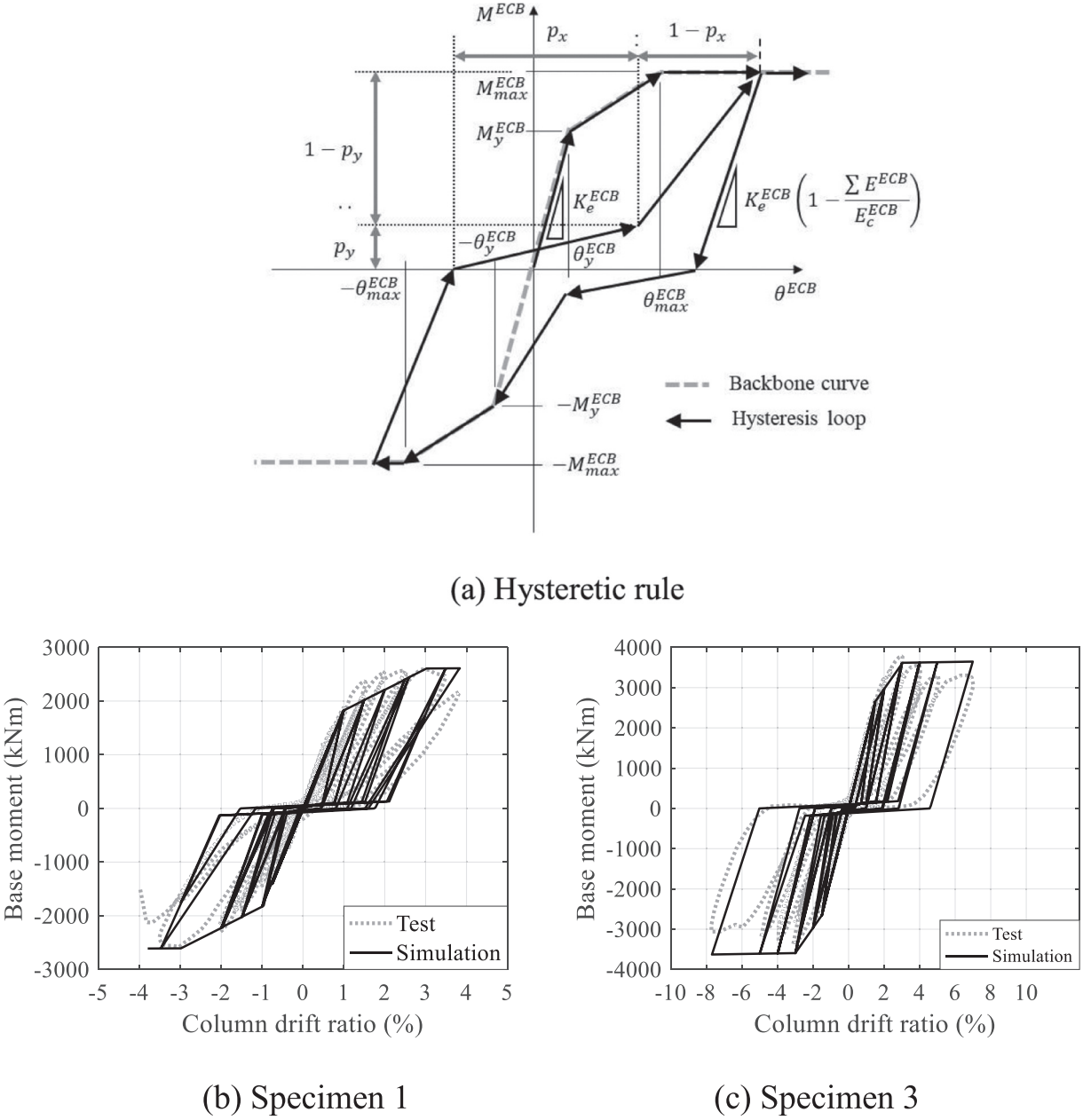

Fig. 6. CFE simulation model and validation with experimental data (test data from [5]).

experimental results is noteworthy in terms of global and local deformation patterns, deduced moment-column drift ratios as well as axial shortening versus column drift ratios regardless of the imposed loading histories.

As noted in Fig. 6, the hysteretic behavior of ECB connections is dominated by pinching and unloading stiffness deterioration due to the concrete bearing failure. Experiments on ECBs by the second author and his former students [5] suggest that the above failure mode within the concrete footing is not strongly influenced by the compressive axial load demand. Consequently, its hysteretic response may be represented through a concentrated hinge model with a pinched behavior as illustrated in Fig. 6a. A similar approach was also adopted in prior studies [39]. Note that local responses (e.g., base plate and concrete) cannot be disaggregated and discussed separately with this modelling approach.

For this purpose, we developed and implemented in the ABAQUS finite element software (version 6.14–1) a user-defined element (UEL). Referring to Fig. 6a, the model follows a trilinear backbone curve including the basic loading, unloading and re-loading paths. These are controlled by two pinching parameters p_x and p_y [40]. The model is able to simulate basic strength and unloading stiffness deterioration based on the energy-based deterioration rule proposed by Rahnama and Krawinkler [40,41] and subsequently modified by Lignos and Krawinkler [42]. This rule assumes that the ECB connection has a reference hysteretic energy dissipation capacity, E_c^{ECB}, which may be estimated as follows,

$$E_c^{ECB} = \lambda^{ECB} \cdot \theta_p^{ECB} \cdot M_y^{ECB} \tag{8}$$

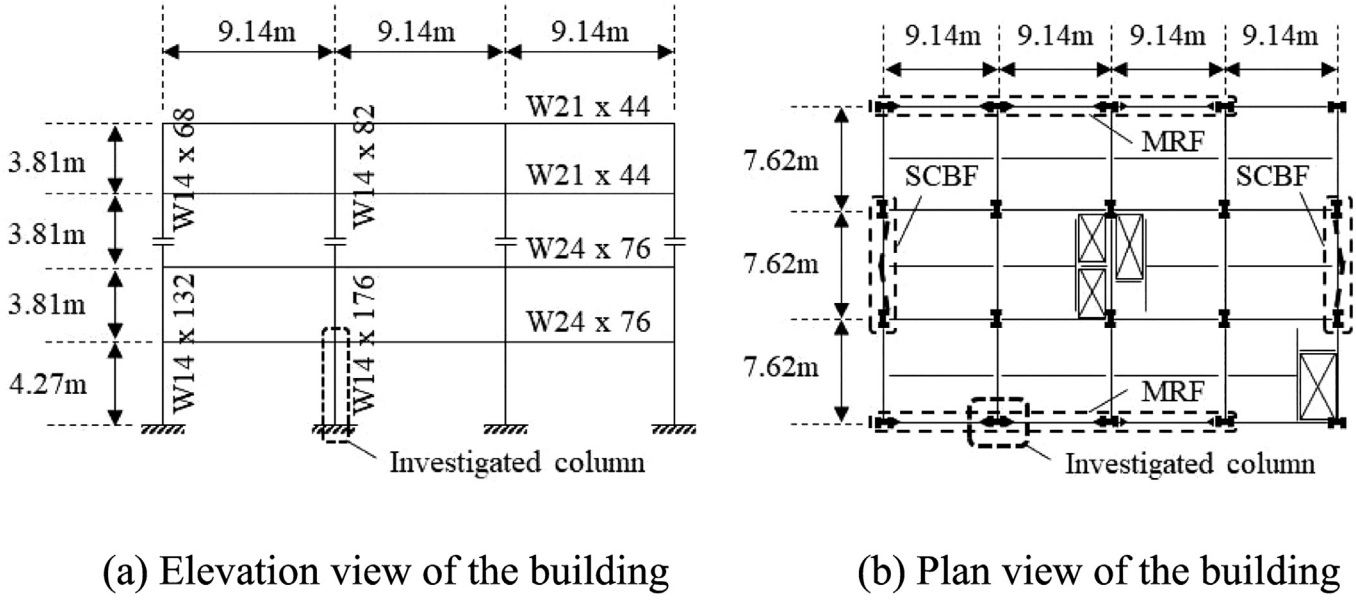

(a) Elevation view of the building (b) Plan view of the building

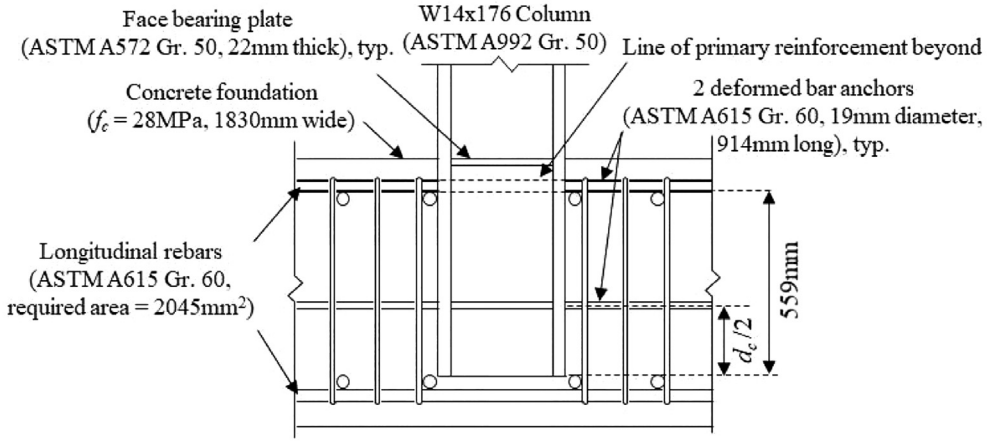

(c) Elevation view of the ECB connection

Fig. 7. Embedded column base design example as adopted from the Seismic Design Manual.

in which, λ_{ECB}, is the reference cumulative rotation capacity, which in turn may be estimated through calibrations with ECB physical tests exhibiting concrete bearing failure.

Fig. 6b and c illustrate comparisons of the simulated versus measured hysteretic response with noteworthy accuracy. Referring to Fig. 6b and c, while flexural strength deterioration may not be evident in the ECB hysteretic response, the primary deteriorating mechanism is associated with unloading stiffness deterioration, which is induced by concrete bearing failure. The cumulative rotation capacity, λ_{ECB} was found to be 2.6 and 25.8 for specimens 1 ($d_{\text{embed}} = 508$ mm) and 3 ($d_{\text{embed}} = 762$ mm), respectively. The corresponding pinching parameters are determined as $p_x = 0.8$, $p_y = 0.05$. These parameters are adopted hereinafter.

4.2. Simulation of a characteristic design case study

The CFE model is used to simulate the hysteretic response of a characteristic design case, which is documented in the AISC Seismic Design Manual [1]. The example features an ECB connection as part of a 4-story 3-bay steel MRF building. Fig. 7a and b illustrates the plan view and elevation of the steel frame building, respectively. Fig. 7c illustrates the final design of a typical first story ECB connection. This is comprised of a 4270 mm long W14x176 steel column. The cross-section profile is made of ASTM A992 Gr. 50 (i.e., nominal yield stress, $f_{y,\,n}$=345 MPa). The steel column is embedded into an RC footing, which is made of 28 MPa concrete. The foundation is reinforced with longitudinal and transverse reinforcing bars such that the concrete bearing becomes the critical failure mode. Furthermore, deformed anchor bars are attached to the embedded column flanges as transfer reinforcement. A base plate is not present in this example. Following the Seismic Design Manual, the column base may be designed for a flexural demand that is the lesser of (a) $1.1ZR_yf_{y,\,n}$ or $(1.1/1.5)ZR_yf_{y,\,n}$, (i.e., R_y, $f_{y,\,n}$, and Z are the ratio of the expected yield stress to the specified minimum yield stress, specified minimum yield stress of steel, and the plastic modulus of the steel column cross section, respectively); and (b) the flexural demand, which is calculated by the load combinations according to [43]. The maximum ECB flexural and shear resistances for the specific design example are found to be, $M_{max}^{ECB} = 1964kNm$, $V_{max}^{ECB} = 921kN$, respectively.

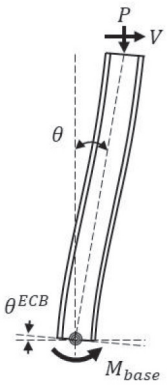

(a) Definitions of primary variables

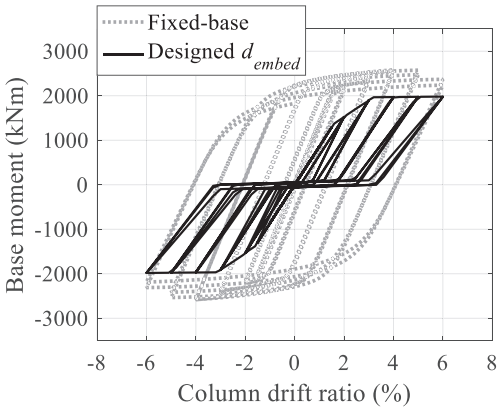

(b) Base moment – column drift ratio (Case I)

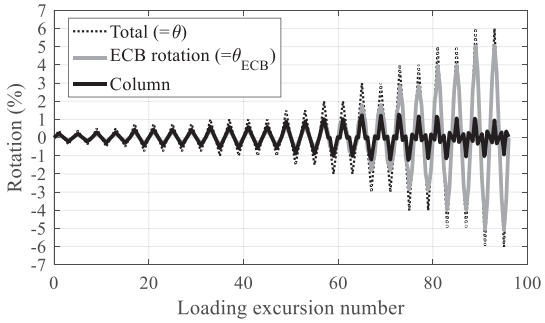

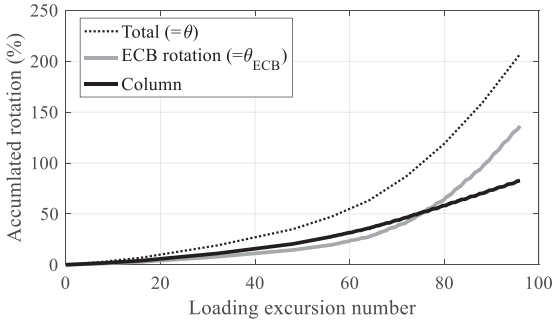

(c) Case I: Contribution of each component to the total and accumulated rotation versus loading excursion

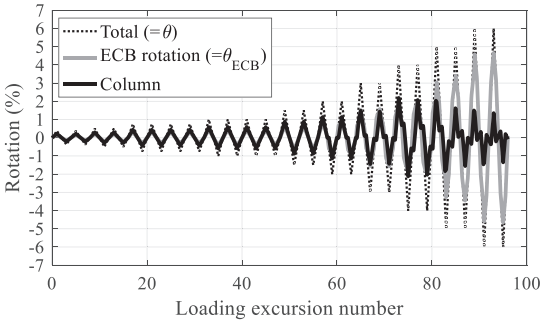

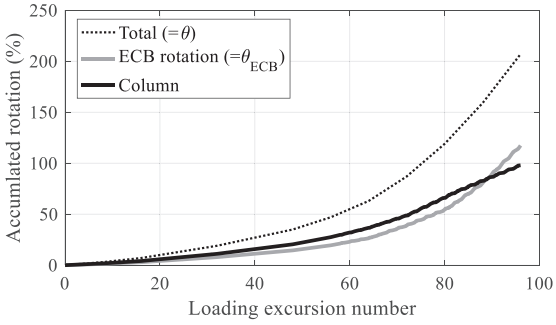

(d) Case II: Contribution of each component to the total and accumulated rotation versus loading excursion

Fig. 8. Base moment – column drift ratio along with the decomposition of the total and accumulated rotations versus the loading excursion.

Notably, according to the current design provisions [22], there is no distinction with regard to the corresponding steel material hardening depending on the steel grade of the column (e.g., A992 Gr. 50 versus A913 Gr. 65). Moreover, the ECB connection may be designed for a moment demand that is smaller than the corresponding plastic flexural resistance of the embedded steel column. The CFE model of the steel column–RC footing subassembly follows the modelling principles presented earlier. At the column top end, the in-plane rotational flexibility of the first-floor beam-to-column connections is explicitly considered. This indicates a more realistic boundary condition of first story steel MRF columns [9,31]. Based on prior work by the authors [5,31], the elastic stiffness of the ECB is estimated to be $5E_sI/L$ of the column (L is the

length of the column). The remaining degrees of freedom in the CFE model are idealized as fixed. To reflect the associated variability of concrete in Eq. (1) with regard to the estimation of the maximum flexural resistance of the ECB connection, three cases are considered, including an "as-designed" case (Case I) with nominal properties and two other cases, where the M_{max}^{ECB}, reflect a 10% and 20% increase compared to the "as designed" case (Case II and Case III, respectively). The corresponding embedment depth, for the ECB to remain elastic, are 559 mm, 615 mm and 671 mm, respectively, for the three cases discussed above.

The steel column-ECB connection subassembly is subjected to the SAC symmetric cyclic loading protocol [44] coupled with a constant compressive axial load that is 9% of the cross-sectional yield load calculated with the expected yield stress as indicated by the design example [1]. Fig. 8 illustrates the simulated results for the 'as-designed' case (Case I) in terms of deduced column base moment, M_{base}, versus column drift ratio as defined in Fig. 8a. The analyzed case is compared with an ideally fixed-base steel column without the presence of the RC foundation (denoted "fixed-base"). Referring to Fig. 8b, the simulation results suggest that the "as designed" case exhibits inelastic behavior in the RC footing rather than the steel column itself. This is clearly seen in Fig. 8c that depicts the decomposition of the total into its subcomponents from the steel column portion and the ECB connection. For lateral drift demands of about 1%, the accumulated rotation between the two components is roughly equal, acknowledging the elastic contribution of the ECB to the total lateral drift. However, above 2% lateral drift demands, the accumulated rotation from the ECB is larger than that of the steel column above the RC footing. Evidently, the current design approach, does not prevent the inelastic behavior within the RC foundation, which is the non-dissipative (and possibly brittle) element in this case. A 10% and 20% increase in the embedment depth of the ECB connection decreases the inelastic contribution of the RC footing as shown in Fig. 8d and e, respectively.

While the mischaracterization of connection capacity is one issue, another key reason for the insufficient design of the ECB connection according to the Design Manual [1] pertains to the fact that the flexural demands on the ECB may exceed the estimated flexural resistance of the steel column itself. The mechanistic reasons of this increase are associated with (a) cyclic hardening which is a function of the material type; (b) cross sectional compactness that controls the onset and progression of local and/or lateral torsional buckling of the steel column; (c) the influence of the loading history that may manifest the material hardening prior to the onset of local buckling; and (d) the axial load demands imposed to the steel column. To determine the relative and interactive contributions of these effects, a parametric study is conducted as outlined in the next section.

Table 2
Virtual test matrix.

Cross section	Web local slenderness (h/t_w)	Steel material	Lateral loading protocol	Axial load protocol
W14x370	6.9	A992 Gr. 50, A913 Gr. 65	SAC symmetric, Collapse consistent	Constant: $P_g/P_y = 5\%$, 20%, 35%, 50%, Variable: $P_g/P_y = 5\%$, 15%, 25%
W24x370	14.2			
W24x229	22.5			
W24x146	33.2			
W24x103	39.2			
W24x84	45.9			

4.3. Parametric study

Using the methodology outlined in the previous sections, a virtual test matrix (see Table 2) is assembled to examine the design space in which ECB connections concentrate their inelastic deformations solely in the steel column right above the RC footing, as implied in capacity designed steel MRFs. While the ECB is assumed to behave elastically in the examined cases, its flexibility is explicitly considered in the CFE model as discussed in [31]. Referring to Table 2, six wide flange steel profiles commonly used in seismic resistant steel MRFs [45,46], are selected. Their web local slenderness ratio, h/t_w, ranges between $7 \le h/t_w \le 46$. Cross sections near the lower bound are unlikely to experience local buckling at high lateral drift demands [47], thereby inducing high flexural demands due to the associated material cyclic hardening. On the other hand, slender cross sections near the current slenderness limits for highly ductile members tend to limit the flexural demands due to the onset of nonlinear geometric instabilities at modest lateral drifts [9,10]. The steel material is either A992 Gr. 50 ($f_{y,\,n}$=345 MPa) or A913 Gr 65 ($f_{y,\,n}$=450 MPa). While the former is a standard choice in seismic resistant steel MRFs, the latter is considering its prospective use in future seismic design. The employed model parameters of the Voce and Chaboche multiaxial plasticity model are based on the modelling by [35,36].

Referring to Table 2, two loading protocols are used: (1) the symmetric SAC symmetric protocol [44,48], which is likely to produce the highest flexural demands, and (2) a collapse-consistent loading protocol [49] that is more representative to be used for the quantification of the seismic demands of ECB connections prior to incipient structural collapse. The lateral loading history is applied in the presence of either a constant compressive axial load, ranging from 5% to 50% of P_y (i.e., axial yield strength of the column based on expected material properties, $P_y = R_y f_{y,\,n} A$), or a time-varying axial load in which the

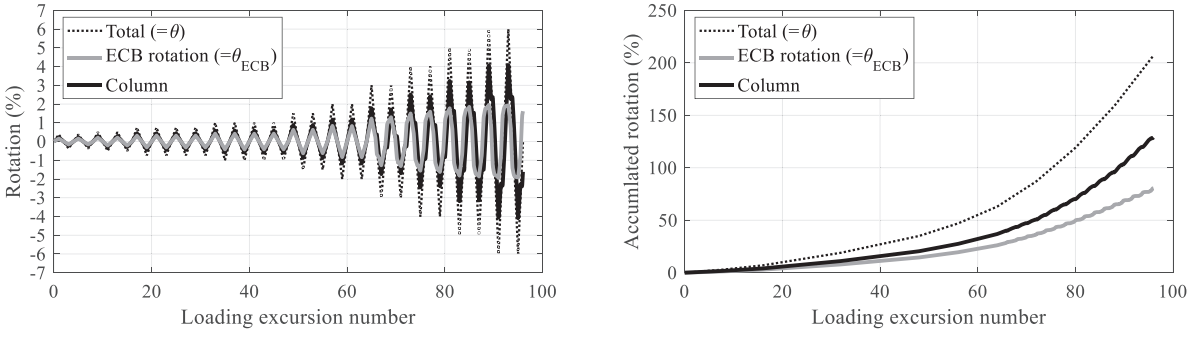

(e) Case III: Contribution of each component to the total and accumulated rotation versus loading excursion

Fig. 8 (*continued*).

steel columns may experience tensile axial loading during a lateral drift excursion. Albeit the former is common in interior columns, the latter is representative in exterior columns due to dynamic overturning effects. The axial load variation is synchronized with the respective lateral loading history as depicted in Fig. 9. This variation is established based on the methodology discussed in [49].

The reduction in the variation of axial load demand is attributed to force redistribution within the overall frame after the onset of geometric instabilities. The steel columns summarized in the virtual test matrix of Table 2, are subjected to progressively increasing loading excursions till their peak flexural strength deteriorates cyclically by at least 20%.

4.4. Results and discussion

Fig. 10 summarizes selected results regarding the influence of each variable on the hysteretic response of steel columns in terms of the column base moment versus the column drift ratio as defined in Fig. 8a. The moment is normalized with respect to the plastic flexural resistance of the respective column cross section. For each case, the maximum attained flexural demand, M_{max}, is extracted and collectively presented in Fig. 11 to establish general trends that inform the prospective development of refined design recommendations for non-dissipative ECB connections. The following observations are made:

- Referring to Fig. 10a and Fig. 11a, steel columns with stocky cross sections (i.e., h/t_w in the range of 7–14) with compressive axial load ratios $P_g/P_y \leq 0.20$, attain a M_{max}/f_yZ ratio of about 1.6. On the other hand, the same ratio, for cross sections near the AISC 341–16 compactness limits (i.e., h/t_w in the range of 33–46) for highly ductile members, does not exceed 1.2. In the latter, the onset of local buckling at modest lateral drift demands tends to inhibit the column's flexural demands as shown in Fig. 10b for two analyzed cases featuring a stocky and slender cross section profiles.
- Referring to Fig. 10c and d, in column cross sections near the AISC 341–16 [22] compactness limits for highly ductile members, when subjected to variable axial load demands, the M_{max}/f_yZ ratio does not exceed 1.2.
- With regard to the steel material (see Fig. 10e), while A913 Gr. 65 steel columns exhibit modest isotropic hardening compared to their A992 Gr. 50 counterparts, the larger kinematic hardening of A913 Gr. 65 further delays the onset of local buckling. However, the

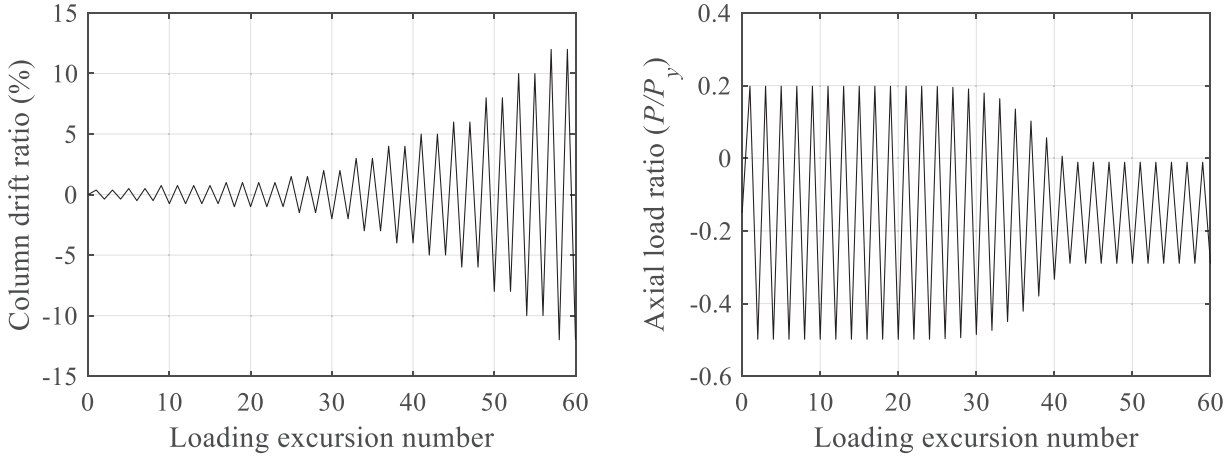

(a) Symmetric cyclic loading history

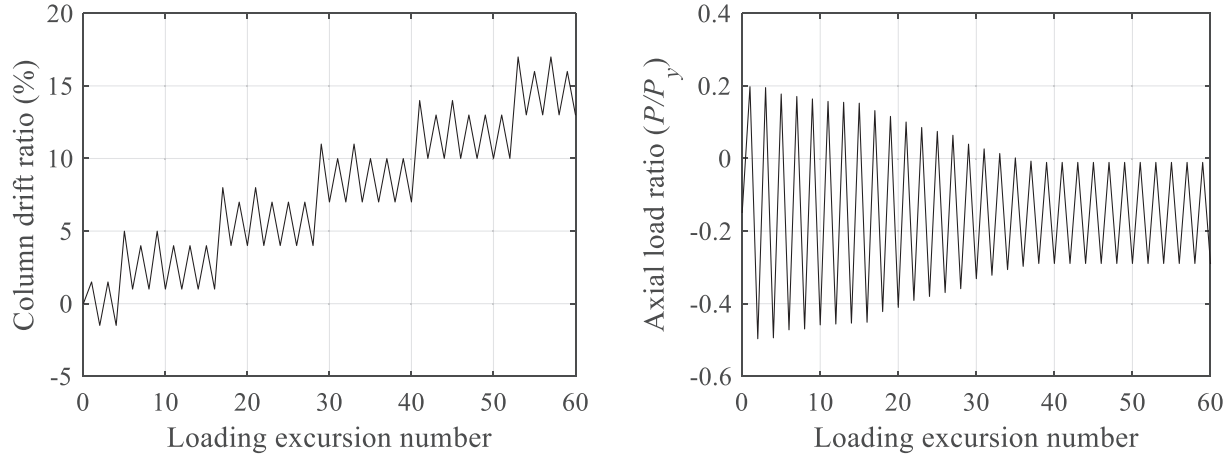

(b) Collapse-consistent loading history

Fig. 9. Lateral and axial loading histories on a W24x146 column with gravity offset, $P_g/P_y = 0.15$ (A992 Gr. 50).

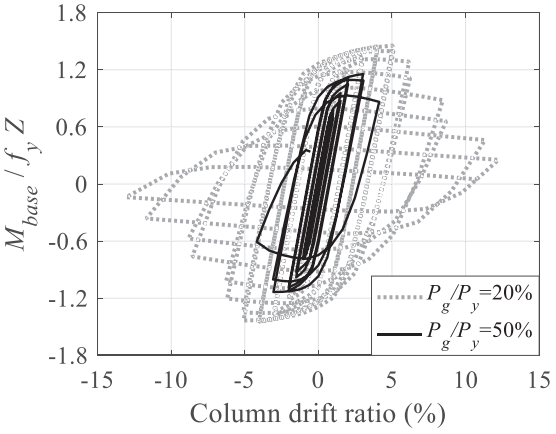

(a) W24x370 (A992 Gr. 50, constant axial load)

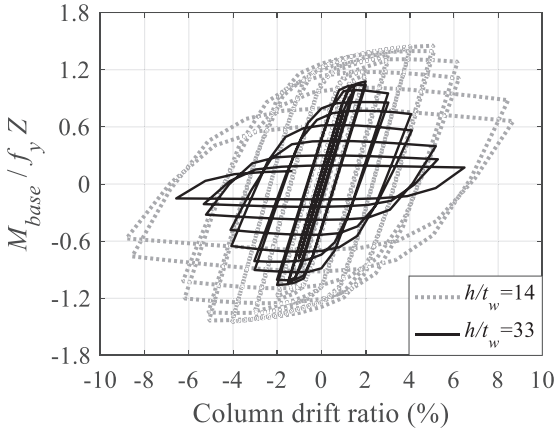

(b) $P_g/P_y = 0.20$, A992. Gr. 50 steel

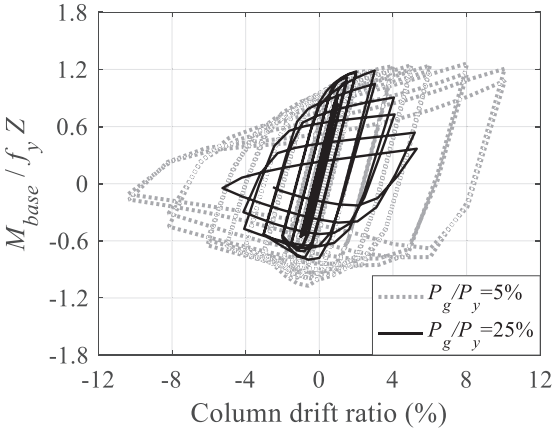

(c) W24x146 (A992 Gr. 50, variable axial load)

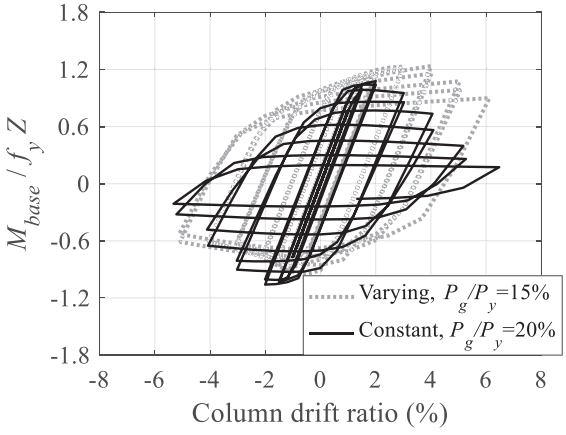

(d) W24x146 (A992 Gr. 50 steel)

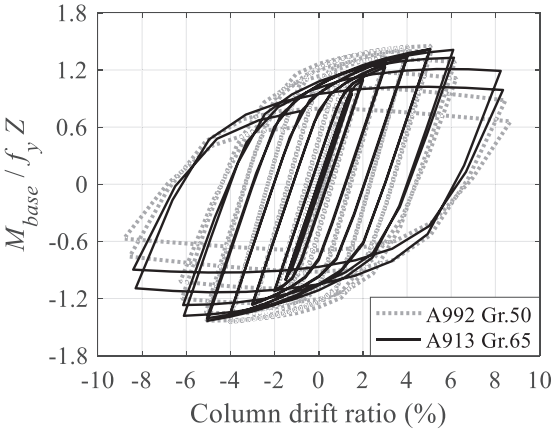

(e) W24x370, $P_g/P_y = 0.20$

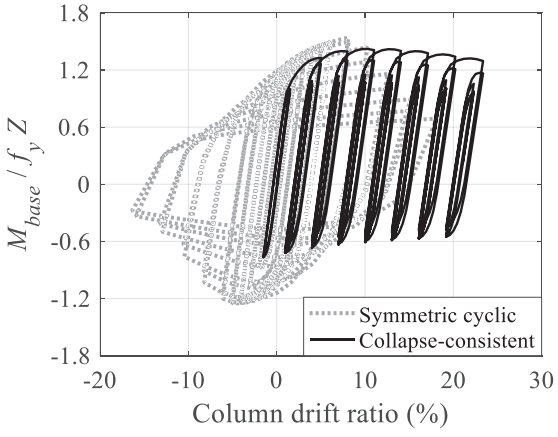

(f) W24x370 (A913 Gr. 65, variable axial load)

Fig. 10. Influence of investigated parameters on the hysteretic response of steel columns

differences with wide-flange profiles made of A992 Gr. 50, in terms of the M_{max}/f_yZ ratio, appear insensitive to the steel material (see Fig. 11a and b).

- Fig. 10f, 11b and d suggest that flexural demands in embedded steel columns are sensitive to the imposed lateral loading history only when (a) they feature stocky cross-sections (i.e., $h/t_w \leq 15$); and (b) they are subjected to time-varying axial load demands. Local buckling-induced softening caps the flexural demands near the ECB connection in all other cases.

4.5. Implications for prospective design

Based on the above discussion, it is noted that the maximum attained flexural demands in capacity-designed steel MRF columns as part of non-dissipative ECB connections are strongly influenced by the steel column position (i.e., interior versus exterior that result in constant versus time-varying axial load), and the cross section geometry (i.e., stocky versus slender profile). The distinction between A913 Gr. 65 and A992 Gr. 50 is statistically insignificant with respect to the corresponding M_{max}/f_yZ ratio based on a standard t-test at the 95% confidence interval. While the imposed lateral and/or axial loading history has a notable influence on the plastic deformation capacity of steel columns, particularly near the incipient collapse limit state, it does not appear to influence the column flexural demands design basis (i.e., probability of exceedance of 10% in 50 years) or maximum considered earthquake (i.e., probability of exceedance of 2% in 50 years) intensity. This is consistent with earlier findings on engineering demand parameters of steel MRFs under seismic loading [50]. Based on these observations, a general regression-based model is suggested to estimate flexural demands in ECB connections in steel MRFs. Particularly, the flexural demand ratio may be estimated as follows,

$$\frac{M_{max}}{f_yZ} = a_0 + a_1 \cdot \left(\frac{h}{t_w}\right) + a_2 \cdot \left(\frac{P_g}{P_y}\right) + \varepsilon \tag{9}$$

In which a_0 is the intercept; a_1 and a_2 are the estimated coefficients of the variables h/t_w and P_g/P_y; ε is the standard error of the predictor. The flange local slenderness ratio, $b_f/2t_f$, is strongly correlated with h/t_w for hot-rolled cross sections manufactured in the United States and Europe [51,52]; hence, $b_f/2t_f$ is excluded from the multivariate regression. However, this assumption may not hold true if built-up cross

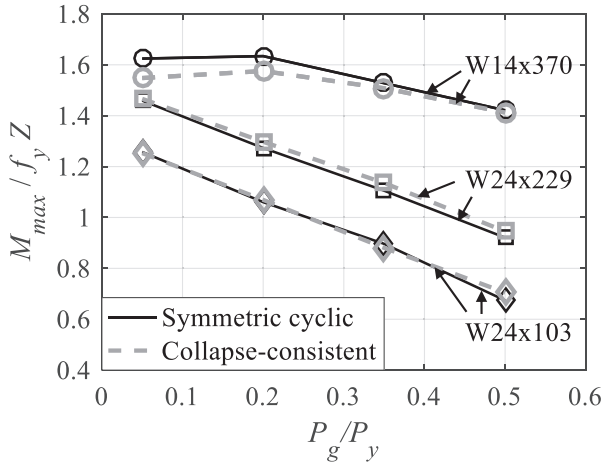

(a) Constant axial load, A992 Gr. 50

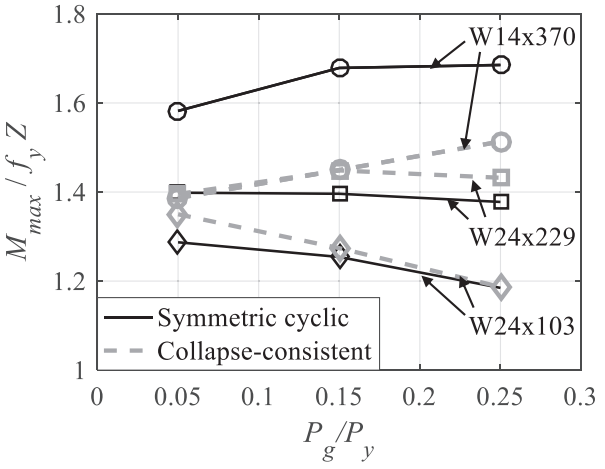

(b) Time-varying axial load, A992 Gr. 50

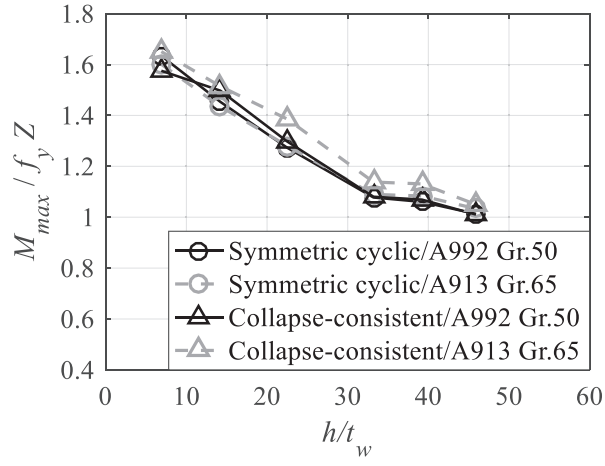

(c) Constant axial load, $P_g/P_y = 0.20$

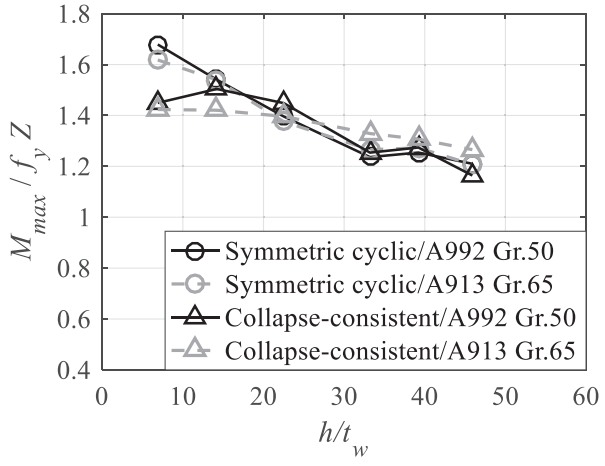

(d) Time-varying axial load, $P_g/P_y = 0.15$

Fig. 11. Representative trends of normalized maximum attained column moment.

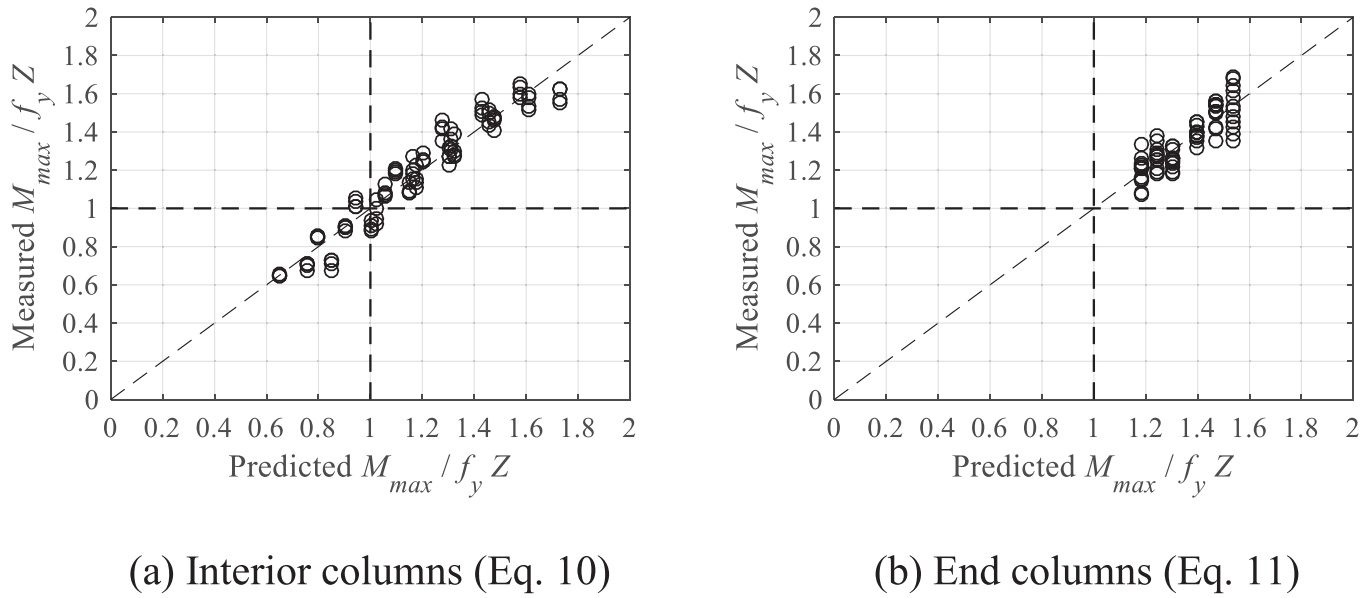

Fig. 12. Measured versus predicted peak flexural strength ratios.

sections (or sections that do not follow this correlation) are employed. The proposed equations are as follows:

Interior steel columns:

$$\frac{M_{max}}{f_y Z} = 1.89 - 0.016 \cdot \left(\frac{h}{t_w}\right) - 0.996\left(\frac{P_g}{P_y}\right),\ R^2 = 0.93,\ COV = 0.07 \quad (10)$$

Exterior steel columns:

$$\frac{M_{max}}{f_y Z} = 1.60 - 0.009 \cdot \left(\frac{h}{t_w}\right),\ R^2 = 0.749,\ COV = 0.05 \quad (11)$$

The range of applicability of Eqs. (10) and (11) is as follows, $7 \le h/t_w \le 46$, and $0 \le P_g/P_y \le 0.5$. For larger web local slenderness ratios (i.e., for the moderately ductile cross-sections), the value corresponding to $h/t_w = 46$ is likely to be conservative. Fig. 12 illustrates the performance of the equations relative to simulation data. Referring to Fig. 12, the accuracy of the proposed formulas for both exterior and interior columns is nearly the same as indicated by the associated COV values of the ratio between the measured and predicted strength quantities. It is evident that the flexural demands in non-dissipative ECB connections may only be smaller than the corresponding plastic flexural resistance of the steel column in cases that the gravity-induced axial load ratio is larger than 20% and the corresponding local web slenderness ratio is $h/t_w \ge 35$. Steel MRFs comprising stocky profiles (e.g., heavy W14) are likely to experience considerable inelastic deformations in their ECB connections with the current design procedure of non-dissipative ECB connections as described in the AISC design manual [1].

Eqs. (10) and (11) may be used to establish lower bound design limits for ensuring elastic response of non-dissipative ECB connections. This may be achieved by designing the ECB connections such that their reliable capacity exceeds the demands implied by Eqs. (10) and (11). From a mechanistic standpoint, this reliable capacity may be determined as, $\phi \cdot M_y^{ECB}$, in which, $\phi = 0.90$, and, $M_y^{ECB} = 0.65 M_{max}^{ECB}$ based on experimental observations by [24]. Particularly, the associated variability mostly comes from the yield stress of the employed steel material. In that respect, this evolves around the expected yield stress of typical A992 Gr. 50 and A913 Gr. 65 steels (i.e., $R_y = 1.1$); thus, $\phi = 0.90$. The associated variability of Eqs. (10) and (11) are fairly minor, as depicted by the relatively small COV values that are reported together with the equations. This is assumed to be the case for the variability due to the actual geometric properties of the steel column as well as the gravitational load demand. The shear demand force may be estimated using the flexural demand derived herein (i.e., $(M_{max} + R_y f_{y,\ n}Z\ )/L$). The axial force demand may be estimated according to the current procedure described in [1]. Similarly, the design procedure according to [1] may be retained to establish the required embedment depth of the ECB connection.

5. Conclusions

This paper presents findings and implications for the seismic design of non-dissipative (or brittle) embedded column base (ECBs) connections as part of capacity designed moment-resisting frames (MRFs). These are based on a rigorous evaluation of the current seismic design models of ECB connections [1,4,22] with past experimental data along with CFE simulations of wide flange steel columns embedded into reinforced concrete (RC) footings. The parametrized CFE model is validated against full-scale experiments of steel columns and ECB connections undergoing highly inelastic deformations due to cyclic loading. The main findings of the study are as follows:

- The AIJ strength design model [4] underestimates the peak flexural resistance of ECB connections, M_{max}^{ECB}, by a factor of two. The AISC design model [1,22] yields more reasonable predictions, but only when the base plate contribution to the overall lateral resistance of the ECB is modest.
- The Grilli and Kanvinde model [24] is fairly accurate in terms of predicting peak flexural strength M_{max}^{ECB}, of the assembled experimental data, excluding cases in which foundation beams are present in the perpendicular loading direction. The additional concrete confinement produced to these beams is unaccounted for in this model.
- The yield ECB flexural resistance, M_y^{ECB} may be estimated as 65% of the maximum attained peak flexural resistance, M_{max}^{ECB}, of an ECB connection. The relatively modest coefficient of variation (i.e., $COV = 0.08$) suggests that the above value is fairly invariant across various configurations.
- The detailed CFE simulations suggest that the AISC [1,22] design approach, unintentionally does not prevent the inelastic behavior of ECB connections within the RC foundation, which is the non-dissipative portion of the ECB connection. This is because flexural

demands commonly estimated in ECB connections do not incorporate the effects of steel material cyclic hardening, cross-sectional slenderness, loading history as well as the imposed column axial load.

- The peak ECB flexural demands normalized with respect to the plastic flexural resistance of the steel column, M_{max}/f_yZ, attain a value of 1.6 when relatively stocky profiles are employed (i.e., $h/t_w < 15$) for gravity-induced axial load ratios of 0.20 or lower (i.e., typical in steel MRFs). The above ratio is capped at 1.2 when slender but still seismically compact profiles are employed in the seismic design process of the ECB connection. Although these observations are detrimental in the context of ECB connections, where the column strength imposes demands on the connection, they may be beneficial in other contexts, e.g., in simulating the proclivity of the frame to sidesway collapse, wherein an increased column strength may delay the formation of soft stories. This is subject to further investigation.
- The CFE results suggest that the M_{max}/f_yZ ratio is practically insensitive to the choice of the material steel grade for the two types of materials that were investigated herein (i.e., A992 Gr. 50 and A913 Gr. 65).
- The seismic demands in ECB connections appear to be sensitive to the loading history only when stocky profiles (i.e., $h/t_w < 15$) are used.

Considering these various effects, simple design equations are proposed to achieve a seismic performance that is more consistent with expectations. The proposed work has several limitations as well, chiefly that experimental data for ECB-column interaction is sparse, necessitating the reliance on simulation. Moreover, a rigorous reliability analysis has not been conducted for the capacity equations, such that the resistance (ϕ-) factors adopted from literature may not be accurate. Furthermore, the ECB strength models (e.g., [24]) are limited by the test details, and extrapolation to significantly different configurations (e.g., with additional footing reinforcement) must be conducted with caution. Finally, the study assumes that the ECB connections are entirely non-dissipative and shall be capacity-designed. While this is consistent with the intent of current design approaches [22], experimental data suggests that ECB connections offer some deformation capacity. Further studies, as well as detailing guidelines for ECB connections may provide methods to leverage this deformation capacity for a more economic design. Notwithstanding these issues (which may be addressed in the future), the proposed approach is likely to yield significantly improved designs in terms of earthquake safety of steel MRFs.

Declaration of Competing Interest

The authors declare that they have no known competing financial interests or personal relationships that could have appeared to influence the work reported in this paper.

Acknowledgements

This study is based on work supported by the Swiss National Science Foundation (Award No. 200021_169248). The financial support is gratefully acknowledged. Any opinions, findings, and conclusions or recommendations expressed in this paper are those of the authors and do not necessarily reflect the views of sponsors.

References

[1] American Institute of Steel Construction (AISC), Seismic Design Manual, Second ed., 2012.
[2] K.A. Harries, D. Mitchell, W.D. Cook, R.G. Redwood, Seismic response of steel beams coupling concrete walls, J. Struct. Eng. 119 (1993) 3611–3629, https://doi.org/10.1061/(ASCE)0733-9445(1993)119:12(3611.
[3] A.H. Mattock, G.H. Gaafar, Strength of embedded steel sections as brackets, ACI J. 79 (1982) 83–93.
[4] Architectural Institute of Japan (AIJ), Recommendations for Design of Connections in Steel Structures, third ed. Architectural Institute of Japan, 2012.
[5] D.A. Grilli, R. Jones, A.M. Kanvinde, Seismic performance of embedded column base connections subjected to axial and lateral loads, J. Struct. Eng. 143 (2017), 04017010. https://doi.org/10.1061/(ASCE)ST.1943-541X.0001741.
[6] G.C. Clifton, M. Bruneau, G.A. MacRae, R. Leon, A. Fussell, Steel structures damage from the Christchurch earthquake series of 2010 and 2011, Bull. N. Z. Soc. Earthq. Eng. 44 (2011) 297–318, https://doi.org/10.5459/bnzsee.44.4.297-318.
[7] G.A. MacRae, G.C. Clifton, M. Bruneau, A.M. Kanvinde, S. Gardiner, Lessons from steel structures in Christchurch earthquakes, 8th International Conference on Behavior of Steel Structures in Seismic Areas (STESSA), Shanghai, China 2015, pp. 1474–1481.
[8] Y. Suzuki, D.G. Lignos, Large scale collapse experiments of wide flange steel beam-columns, Proceedings of the 8th International Conference on Behavior of Steel Structures in Seismic Areas (STESSA), Shanghai, China, 2015.
[9] A. Elkady, D.G. Lignos, Full-scale testing of deep wide-flange steel columns under multiaxis cyclic loading: loading sequence, boundary effects, and lateral stability bracing force demands, J. Struct. Eng. 144 (2018), 04017189. https://doi.org/10.1061/(ASCE)ST.1943-541X.0001937.
[10] G. Ozkula, J. Harris, C.-M. Uang, Observations from cyclic tests on deep, wide-flange beam-columns, Eng. J. 1 (2017) 45–59.
[11] A. Elkady, D.G. Lignos, Improved seismic design and nonlinear modeling recommendations for wide-flange steel columns, J. Struct. Eng. 144 (2018), 04018162. https://doi.org/10.1061/(ASCE)ST.1943-541X.0002166.
[12] J. Cravero, A. Elkady, D.G. Lignos, Experimental evaluation and numerical modeling of wide-flange steel columns subjected to constant and variable axial load coupled with lateral drift demands, J. Struct. Eng. 146 (2020), 04019222. https://doi.org/10.1061/(ASCE)ST.1943-541X.0002499.
[13] H. Akiyama, M. Kurosawa, N. Wakuni, I. Nishimura, Strength and deformation of column bases embedded in base concrete, J. Struct. Construct. Eng. (Transactions of AIJ) (1984) 45–53(In Japanese).
[14] K. Minami, Y. Nishimura, K. Kurisawa, Research on Stress Transfer Mechanism of Embedded Column Base Connection, Summary of Technical Papers of Annual Meeting, Kinki Branch, 1982 293–296.
[15] K. Morita, B. Kato, A. Tanaka, N. Fujita, Experiments investigation on maximum strength of embedded column bases, J. Struct. Construct. Eng. (Transactions of AIJ) (1985) 65–74(In Japanese).
[16] S. Nakashima, S. Igarashi, Behavior of steel square tubular column bases for interior columns embedded in concrete footings under bending moment and shearing force part 1: test program and load-displacement relationships, J. Struct. Construct. Eng. (Transactions of AIJ) (1986) 106–118(In Japanese).
[17] S. Nakashima, S. Igarashi, Behavior of steel square tubular column bases for interior columns embedded in concrete footings under bending moment and shearing force: part 2 initial stiffness, ultimate strength and mechanism of stress flow, J. Struct. Construct. Eng. (Transactions of AIJ) (1987) 63–76(In Japanese).
[18] T. Takeda, Y. Takahashi, Experimental Study on the Column Base of Steel Structure and Steel Reinforced Concrete Structure Part 1: Comparison of 4 Types of Column Bases, Summary of Technical Papers of Annual Meeting, Kanto Branch (In Japanese), 1980 265–268.
[19] T. Takeda, Y. Takahashi, Experimental Study on the Column Base of Steel Structure and Steel Reinforced Concrete Structure Part 2: Examination of the Interior Embedded Column Bases, Summary of Technical Papers of Annual Meeting, Kanto Branch (In Japanese), 1982 229–232.
[20] S. Tsujioka, K. Inoue, K. Imai, M. Hirayama, Strength of improved embedded RHS exterior column-footing connections with U-reinforcing bars, J. Struct. Construct. Eng. (Transactions of AIJ) (In Japanese) 401 (1989) 117–127.
[21] K. Washio, T. Suzuki, S. Nakashima, I. Nishimura, Effect of embedment on the steel column base I part 1: Experimental results, Summary of Technical Papers of Annual Meeting, AIJ, C-1(II) (In Japanese), 53, 1978, pp. 1289–1290.
[22] American Institute of Steel Construction (AISC), Seismic Provisions for Structural Steel Buildings. ANSI/AISC 341–16, American Institute of Steel Construction, 2016.
[23] American Concrete Institute (ACI), Building Code Requirements for Structural Concrete and Commentary. ACI 318–14, American Concrete Institute, 2014.
[24] D.A. Grilli, A.M. Kanvinde, Embedded column base connections subjected to seismic loads: strength model, J. Constr. Steel Res. 129 (2017) 240–249. http://www.sciencedirect.com/science/article/pii/S0143974X1630284X.
[25] G.G. Deierlein, T.M. Sheikh, J.A. Yura, J.O. Jirsa, Beam-column moment connections for composite frames: part 2, J. Struct. Eng. 115 (1989) 2877–2896, https://doi.org/10.1061/(ASCE)0733-9445(1989)115:11(2877).
[26] T.M. Sheikh, G.G. Deierlein, J.A. Yura, J.O. Jirsa, Beam-column moment connections for composite frames: part 1, J. Struct. Eng. 115 (1989) 2858–2876, https://doi.org/10.1061/(ASCE)0733-9445(1989)115:11(2858.
[27] K. Washio, T. Suzuki, S. Nakashima, I. Nishimura, Effect of embedment on the steel column base I part 2: Observations, Summary of Technical Papers of Annual Meeting, AIJ, C-1(II) (In Japanese), 53, 1978, pp. 1291–1292.
[28] N. Barnwell, Experimental Testing of Shallow Embedded Connections between Steel Columns and Concrete Footings, All Theses and Dissertations http://scholarsarchive.byu.edu/etd/4428 2015.
[29] B. Gong, B.M. Shahrooz, Steel-concrete composite coupling beams - behaviors and design, Eng. Struct. 23 (2001) 1480–1490, https://doi.org/10.1016/S0141-0296(01)00042-6.
[30] ABAQUS, ABAQUS Analysis User's Manual Version 6.14–1, Dassault Systems Simulia Corp, RI, USA, 2014.
[31] H. Inamasu, A.M. Kanvinde, D.G. Lignos, Seismic stability of wide-flange steel columns interacting with embedded column base connections, J. Struct. Eng. 145 (2019), 04019151. https://doi.org/10.1061/(ASCE)ST.1943-541X.0002410.
[32] A. Elkady, D.G. Lignos, Analytical investigation of the cyclic behavior and plastic hinge formation in deep wide-flange steel beam-columns, Bull. Earthq. Eng. 13 (2015) 1097–1118, https://doi.org/10.1007/s10518-014-9640-y.

[33] J. Lemaitre, J.-L. Chaboche, Mechanics of Solid Materials, Cambridge university press, 1994.
[34] E. Voce, The relationship between stress and strain for homogeneous deformation, J. Inst. Met. 74 (1948) 537–562.
[35] A. de Castro e Sousa, Y. Suzuki, D.G. Lignos, Consistency in solving the inverse problem of the Voce-Chaboche constitutive model for plastic straining, J. Eng. Mech. 146 (9) (2020) 04020097, https://doi.org/10.1061/(ASCE)EM.1943-7889.0001839.
[36] A. de Castro e Sousa, D.G. Lignos, On the inverse problem of classic nonlinear plasticity models-An application to cyclically loaded structural steels, Resilient Steel Structures Laboratory (RESSLab), Ecole Polytechnique Fédérale de Lausanne, Lausanne, 2017.
[37] B.W. Young, Residual stresses in hot-rolled sections, International Colloquium on Column Strength, International Association for Bridge and Structural Engineering, Zurich, Switzerland 1971, pp. 25–38.
[38] A. de Castro e Sousa, D.G. Lignos, Residual Stress Measurements of European Hot-Rolled I-Shaped Steel Profiles, Resilient Steel Structures Laboratory, École Polytechnique Fédérale de Lausanne (EPFL), Lausanne, Switzerland, 2017.
[39] P. Torres-Rodas, F. Zareian, A. Kanvinde, A hysteretic model for the rotational response of embedded column base connections, Soil Dyn. Earthq. Eng. 115 (2018) 55–65, https://doi.org/10.1016/j.soildyn.2018.08.015.
[40] L.F. Ibarra, R.A. Medina, H. Krawinkler, Hysteretic models that incorporate strength and stiffness deterioration, Earthq. Eng. Struct. Dyn. 34 (2005) 1489–1511, https://doi.org/10.1002/eqe.495.
[41] M. Rahnama, H. Krawinkler, Effects of Soft Soil and Hysteresis Model on Seismic Demands, John A. Blume Earthquake Engineering Center Stanford, 1993.
[42] D.G. Lignos, H. Krawinkler, Deterioration modeling of steel components in support of collapse prediction of steel moment frames under earthquake loading, J. Struct. Eng. 137 (2011) 1291–1302, https://doi.org/10.1061/(ASCE)ST.1943-541X.0000376.
[43] American Society of Civil Engineers (ASCE), Minimum Design Loads and Associated Criteria for Buildings and other Structures. ASCE/SEI 7–16, American Society of Civil Engineers, 2016.
[44] H. Krawinkler, A. Gupta, R. Medina, N. Luco, Development of Loading Histories for Testing of Steel Beam-to-Column Assemblies, Stanford University, 2000.
[45] A. Elkady, D.G. Lignos, Modeling of the composite action in fully restrained beam-to-column connections: implications in the seismic design and collapse capacity of steel special moment frames, Earthq. Eng. Struct. Dyn. 43 (2014) 1935–1954, https://doi.org/10.1002/eqe.2430.
[46] National Institute of Standards and Technology (NIST), Evaluation of the FEMA P695 Methodology for Quantification of Building Seismic Performance Factors, NEHRP consultations Joint Venture, 2010.
[47] J. Newell, C.-M. Uang, Cyclic behavior of steel wide-flange columns subjected to large drift, J. Struct. Eng. 134 (2008) 1334–1342, https://doi.org/10.1061/(ASCE)0733-9445(2008)134:8(1334).
[48] P. Clark, K. Frank, H. Krawinkler, R. Shaw, Protocol for Fabrication, Inspection, Testing and Documentation of Beam-Column Connection Tests and Other Experimental Specimens, 1997.
[49] Y. Suzuki, D.G. Lignos, Development of collapse-consistent loading protocols for experimental testing of steel columns, Earthq. Eng. Struct. Dyn. 49 (2020) 114–131, https://doi.org/10.1002/eqe.3225.
[50] D.G. Lignos, C. Putman, H. Krawinkler, Application of simplified analysis procedures for performance-based earthquake evaluation of steel special moment frames, Earthquake Spectra 31 (2015) 1949–1968, https://doi.org/10.1193/081413EQS230M.
[51] D.G. Lignos, A.R. Hartloper, A. Elkady, G.G. Deierlein, R. Hamburger, Proposed updates to the ASCE 41 nonlinear modeling parameters for wide-flange steel columns in support of performance-based seismic engineering, J. Struct. Eng. 145 (2019), 04019083. https://doi.org/10.1061/(ASCE)ST.1943-541X.0002353.
[52] D.G. Lignos, A.R. Hartloper, Steel column stability and implications in the seismic assessment of steel structures according to Eurocode 8 part 3, Stahlbau 89 (2020) 16–27, https://doi.org/10.1002/stab.201900108.